Conformation of Formacetal and 3′-Thioformacetal Nucleotide Linkers and Stability of Their Antisense RNA·DNA Hybrid Duplexes†

Jeffrey S. Rice and Xiaolian Gao*

Department of Chemistry, University of Houston, Houston, Texas 77204-5641

Received July 17, 1996; Revised Manuscript Received October 10, 1996⊗

ABSTRACT: This study focuses on the characterization of the stability and conformation of the antisense oligodeoxyribonucleotides, d[CGCGTT×TTGCGC] [× = phosphodiester (-O-P(O)$_2$-O-), formacetal (FMA, -O-CH$_2$-O-), or 3′-thioformacetal linkage (TFMA, -S-CH$_2$-O-)], in DNA·DNA and RNA·DNA duplexes (designated DI−III and RI−III, respectively). NMR analysis of two RNA·DNA hybrid duplexes containing a single FMA (the RII duplex) or 3′-TFMA (the RIII duplex) modification has been carried out. The conformations of these duplexes are compared with that of the unmodified hybrid duplex RI and with those of the DI−III duplexes. These analyses and comparisons indicate that the residue containing a 3′-FMA linker has a preference for the C2′-endo sugar pucker and adopts a canonical backbone conformation. In contrast, the residue containing a 3′-TFMA linker has a much increased preference for the C3′-endo sugar pucker and adopts different backbone conformations in the DNA·DNA and RNA·DNA duplexes. UV and NMR melting studies of the six duplexes demonstrate that the DNA·DNA duplexes are more stable than the corresponding RNA·DNA hybrid duplexes and that both FMA and 3′-TFMA destabilize the duplex. The 3′-TFMA modified duplex is less stable than the FMA duplex in the context of DNA·DNA recognition and is slightly more stable than the FMA hybrid duplex in the context of RNA·DNA recognition. These results suggest a correlation between the conformational preference of backbone modifications and the stability of antisense duplexes. The implications of these studies for optimized incorporation of FMA and 3′-TFMA linkers into oligonucleotides and for better design of antisense oligonucleotide analogs are discussed.

The use of antisense oligodeoxyribonucleotides (ODNs) to regulate gene products through complementary binding to mRNA targets has attracted intense research effort (Zamecnik & Stephenson, 1978; Sanghvi & Cook, 1993; Wagner, 1994; Agrawal & Iyer, 1995). The success of antisense ODNs relies on their stable duplex formation with targeted RNA to block specific gene regulation sites or to induce RNA cleavage by RNase H at the binding site (Reynolds *et al*., 1996). To further the progress in this field, it is of fundamental importance to understand the molecular basis of binding affinity and sequence specificity achievable by ODN recognition of RNA sequences. Such knowledge would permit the development of antisense ODN analogs which possess improved chemical and biological properties. Although examples abound for successful application of antisense strategy to gene regulation *in vitro* (Minshull & Hunt, 1992; Liebhaber *et al*., 1992), *in vivo* antisense applications have been limited by problems associated with ODNs containing natural, phosphodiester backbones. These molecules do not readily diffuse across the lipophilic cell membrane, and the molecules that do enter the cell are likely to be rapidly degraded by nucleases, especially by 3′-exonucleases, or they are trapped in vacuoles within the cells before reaching their targets (Tidd & Warenius, 1989; Woolf *et al*., 1990; Shaw *et al*., 1991; Hoke *et al*., 1991; Shoji *et al*., 1991). These difficulties prevent the accumulation of sufficiently high cellular concentrations of phosphodiester ODNs to achieve an effective antisense response.

Several strategies have been adopted to circumvent the instability and importation problems of natural ODNs. For instance, many of these strategies involve the use of terminal lipophilic capping groups or conjugation chemistry (Manoharan, 1993; Sinyakov *et al*., 1995) or modification of base and sugar residues (Uhlmann & Peyman, 1990; Sanghvi 1993; Sanghvi & Cook, 1994). Substantial progress has been made toward successful backbone modifications (Uhlmann & Peyman, 1990; Sanghvi & Cook, 1993), using phosphorous (phosphorothioates and methylphosphonates) or non-phosphorous groups possessing a wide range of bond geometry and polarity. The backbone properties (nuclease resistance, stability, and cell permeability) are determined by the substituent groups and the chirality of the various linker moieties. While some of these modified backbone linkages are highly resistant to nuclease degradation (Helene & Toulme, 1990; Chiang *et al*., 1991), many still suffer from an inability to reach their RNA targets or from low binding affinity to target RNA sites (Bennett *et al*., 1992; Ceruzzi *et al*., 1990; Shoji *et al*., 1991). A number of achiral and neutral backbone designs, such as peptide−nucleic acids (Nielsen *et al*., 1991), methylhydroxylamine linkers (Vasseur *et al*., 1992; Sanghvi & Cook, 1993), and formacetal derivatives (Matteucci, 1990) have been reasonably successful in binding properties and in *in vitro* experiments, demonstrating the potential of achiral and neutral backbone modifications in developing effective antisense agents.

† This research is supported by NIH (R29 GM49957-01). The 600 MHz NMR spectrometer at the University of Houston is funded by the W. M. Keck Foundation.

* To whom correspondence should be addressed. Tel: (713) 743-2805. FAX: (713) 743-2709. E-mail: gao@kitten.chem.uh.edu.

⊗ Abstract published in *Advance ACS Abstracts,* December 15, 1996.

S0006-2960(96)01760-6 CCC: $14.00

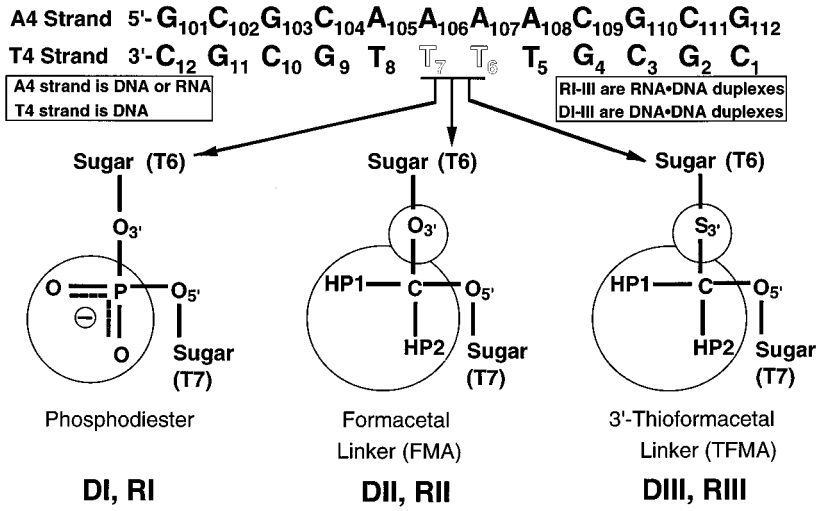

FIGURE 1: Sequences of the antisense duplexes studied. The unmodified top strand is either DNA or RNA to give six DI−III and RI−III duplexes. The formacetal or 3′-thioformacetal linkers are located between T6 and T7 of the DNA strand. HP1 and HP2 are the methylene protons of the formacetal or 3′-thioformacetal linkers.

The rapid development in chemical synthesis and biological studies of antisense ODN analogs has led to a library of molecules with characteristic properties. This progress offers an opportunity to examine, at atomic resolution, a related group of modified ODNs in a systematic manner and to characterize the function of these modified chemical moieties in nucleic acid recognition (Brown *et al*., 1994; Gonzalez *et al*., 1994, 1995; Cummins *et al*., 1996; Eriksson & Nielsen, 1996). Although presently the design of the modified antisense ODN analogs is based mainly on empirical derivation and qualitative chemical and structural knowledge, the accumulation of structural and dynamics information on antisense ODNs should gradually enhance the role of objective design by molecular modeling. There are several important questions to be probed concerning the design of antisense ODNs. For instance, what is the correlation of the binding properties of antisense ODNs with the type of chemical modifications or functional groups? What is the molecular basis for the observed correlation? What is the conformation of the lowest energy state for local modification sites and for duplex formation, and are there major differences between these conformations and the structures of natural sequences? What is the effect due to differences in sequence, position and number of modification sites?

Our investigation of antisense ODNs has been focused on the neutral and achiral formacetal (FMA)[1] and 3′-thioformacetal (3′-TFMA or TFMA) backbone linker modifications (Matteucci, 1990; Jones *et al*., 1993) in comparison with natural phosphodiester linkages. A single linker is incorporated into DNA dodecamers, between two thymidine (T) residues located in the center of the sequence (Figure 1). The modified DNA strands are annealed to the complementary DNA or RNA strands, resulting in two FMA modified duplexes DII (complementary DNA strand) and RII (complementary RNA strand) and two 3′-TFMA modified duplexes DIII (complementary DNA strand) and RIII (complementary RNA strand). The unmodified RNA·DNA (RI) and DNA·DNA (DI) duplexes containing phosphodiester linkages are used as a reference system. We are using this system to characterize the FMA and 3′-TFMA linkers in the context of RNA·DNA or DNA·DNA duplexes in an effort to address the questions presented above.

NMR studies of the FMA-containing DNA·DNA duplex (DII, T6-OCH_2O-T7) demonstrated that the structural adjustments are localized at the modification site and are minimal relative to the unmodified DI duplex (Gao *et al*., 1992). A close comparison indicates that the T6 sugar of DII contains slightly more C2′-endo type pucker than the T6 sugar of DI. In contrast, the 3′-TFMA-containing DNA·DNA duplex (DIII, T6-SCH_2O-T7), which differs from DII only by one atom ($T6_{O3'} \rightarrow T6_{S3'}$), exhibits substantial structural adjustment in T6 sugar pucker and in the backbone angles linking T6 and T7 residues. The T6 sugar pucker is averaging between C2′- and C3′-endo conformations, appearing as an intermediate, averaged conformation (Gao & Jeffs, 1994a). The variations in linker backbone angles are revealed by a set of unusual NOEs involving the linker methylene protons of the DIII duplex. The theoretical basis for the observations mentioned above was explored by Veal *et al*. using quantum mechanics and molecular dynamics calculations (Veal *et al*., 1993; Veal & Brown, 1995). These calculations led to the generation of a B-type conformation for the FMA linker and an unusual conformation for the TFMA linker in a TT dimer, in agreement with NMR results (Gao *et al*., 1992; Gao & Jeffs, 1994a).

In the following, we report the NMR analysis of two RNA·DNA hybrid duplexes containing a single FMA (RII) or 3′-TFMA (RIII) modification (Figure 1) and their comparison with the unmodified hybrid duplex RI, whose conformational analysis has been described previously (Gao & Jeffs, 1994b). In addition, UV and NMR melting studies have been carried out on all six duplexes (DI−III and RI−III) under identical solvent and sample conditions. The comparison of these results focuses on: (a) the overall structural features and the relative stability of the six duplexes; (b) the conformations of the FMA linker and the TFMA linker in the RNA·DNA hybrid duplexes (*i.e*., the comparison between the residues at the linker site in RII

[1] Abbreviations: 1D, one-dimensional; 2D, two-dimensional; FMA, formacetal; 3′-TFMA, 3′-thioformacetal; COSY, correlation spectroscopy; DQF, double quantum filter; J-R, jump-return pulse sequence; NMR, nuclear magnetic resonance; NOE, nuclear Overhauser effect; NOESY, nuclear Overhauser effect and exchange spectroscopy; T_m, melting temperature; UV, ultraviolet; TOCSY, total correlation spectroscopy.

and RIII and those in the unmodified RI); (c) the local conformation of the FMA and TFMA linkers in an RNA·DNA hybrid duplex *versus* in a DNA·DNA duplex (*i.e*., the comparisons of the conformation of a linker in different environments, represented by DII *versus* RII or DIII *versus* RIII); (d) the structural effect of the antisense strand binding on the RNA strand *versus* on the DNA strand (*i.e*., the comparisons among the unmodified strands in RI, RII and RIII). These NMR results have been used to elucidate the 3D structure of the RIII duplex using molecular dynamics simulations. The analysis of the high-resolution structural information has been completed and will be reported separately (Cross *et al*., 1996).

MATERIALS AND METHODS

Sample Preparation

The FMA-containing d[CGCGTT-OCH$_2$O-TTGCGC] and 3′-TFMA-containing d[CGCGTT-SCH$_2$O-TTGCGC] strands were provided by Gilead Sciences and Glaxo Pharmaceuticals, Inc. The unmodified DNA strands, d[CGCGTTTTG-CGC] and d[GCGCAAAACGCG], were synthesized using solid phase phosphoramidite protocols and purified as reported in the literature (Gao *et al*., 1992). The RNA strand, r[GCGCAAAACGCG], was either obtained from Glaxo or synthesized on a Cruachem PS250 DNA/RNA synthesizer using phosphoramidite chemistry. The synthesis was carried out on a 1 μmol scale and the 1-(2-fluorophenyl)-4-methoxypiperidin-4-yl (Fpmp) was used as the O2′ protecting group (Beijer *et al*., 1990; Capaldi & Reese, 1994). Treatment in concentrated NH_4OH at 55 °C for 14 h cleaved the RNA oligonucleotide from the solid support resin and removed base-sensitive protecting groups, while the 5′-(4,4′-dimethoxytrityl) and the O2′-Fpmp were untouched. The 5′-trityl-positive RNA strand was isolated using a Waters RCM C_{18} HPLC column (10 × 25 cm) and eluted using the following gradients: 2−35% B in 5 min; hold at 35% B for 20 min; 35−55% B in 40 min. The flow rate of the mobile phase was 4 mL/min, and mobile phase A = 0.1 M TEAA aqueous solution, pH 6.7, and B = CH_3CN. The fractions containing the full-length RNA strand were concentrated by freeze-drying. The O2′-Fpmp and 5′-trityl groups were removed by incubation in a sodium acetate buffer at pH 3.25 (Cruachem) for 30 h at ambient temperature with constant agitation. The reaction mixture was neutralized with a 1 M tris(hydroxymethyl)aminomethane (TRIS) buffer (Cruachem) and concentrated by freeze-drying. The dried sample was dissolved in H_2O and applied to the C_{18} column and eluted using the following gradients: 2−10% B in 5 min; hold at 10% B for 35−40 min until the peak of interest eluted. The flow rate and mobile phases were the same as described above. The fractions of interest were lyophilized and then dissolved in H_2O. The final RNA strand product was desalted on size-exclusion (Bio-Rad, PG-60) and sodium exchange (Aldrich, Dowex-50-hydrogen) columns eluted with H_2O.

For NMR experiments, all six duplexes used in this study were dissolved in 0.1 M NaCl, 10 mM sodium phosphate, and 0.1 mM sodium EDTA using D_2O (99.96%, Cambridge Isotopes, Inc.) as the solvent for observation of non-exchangeable protons, or 90% H_2O−10% D_2O as the solvent for observation of exchangeable protons. The pH values were in the range of 5−7 (accurate to ±0.1 units), and those reported in D_2O were uncorrected pH meter readings. The final NMR samples contained 1−2 mM concentrations of the duplexes.

NMR Experiments

All NMR experiments were conducted on a Bruker AMXII 600 MHz spectrometer. Proton chemical shifts were referenced to the HOD resonance (4.70 ppm at 25 °C, temperature correction factor −0.0109 ppm/°C). NMR data were processed using the UXNMR program (Bruker Instruments, Inc.) and the FELIX 2.30 program (Molecular Simulations, Inc.).

One-Dimensional Experiments of DI−III and RI−III. The annealing of the modified DNA strands with their complementary RNA strand were monitored by one-dimensional (1D) proton spectra at room temperature. The non-selective spin−lattice relaxation times, T_1, were estimated from the null point in D_2O solution at 25 °C using an inversion recovery pulse sequence (Freeman *et al*., 1980) and 15 s repetition delays. The results demonstrate that the longest T_1 values, belonging to the adenine H2 protons, are less than 3.9 s and that most T_1 values are less than 2.9 s. In 90% H_2O solution, T_1 values are shorter by ∼30%.

Imino proton temperature dependent experiments for all six duplexes were performed with ∼1 mM duplex in pH 6.2 H_2O buffer. The spectra were obtained using the jump-return (J-R) pulse sequence, for HOD suppression, with maximum excitation frequency centered at ∼12.8 ppm (Plateau & Gueron, 1982). Temperature increments/decrements ranged from one to eight degrees and were separated by a minimum of 10 min of equilibration time. The time domain data of these 1D temperature dependence experiments consisted of 8192 complex data points over a sweep width of 13.5 kHz. The NMR melting curves were obtained by plotting the line widths, at half peak height, of well-resolved imino proton resonances as a function of temperature (Supporting Information, Figure S1). The imino protons of T5 and G9 for the hybrid duplexes (RI−III) and those of T8 and G9 for the DNA·DNA duplexes (DI−III) are well-resolved and are used as measurement markers.

Two-Dimensional NMR Experiments of RII and RIII. Two-dimensional (2D) NMR spectra of hybrid duplexes, RII and RIII, were collected with a sample concentration of 2 mM. Most 2D NMR data were obtained with simultaneous detection in t_2 and TPPI phase cycling (Marion *et al*., 1983) in t_1 dimension. The States−Ruben−Haberkorn phase program (States *et al*., 1982) was used for the COSY-35 and $^1H-^{31}P$ correlation spectra. The 2D NOESY spectra of exchangeable protons were acquired at 15 °C (1.3 s relaxation delay, 100 and 150 ms mixing times, 13.5 kHz spectral window, and 4096 × 512 data size). The strong H_2O signal was suppressed using the J-R pulse sequence with a refocus delay of 53 μs. 2D NOESY spectra of non-exchangeable protons (4.6 s relaxation delay, 70, 140, 200 and 250 ms mixing times, 5.1 kHz spectral window, and 2048 or 4096 × 512 data size) were acquired at 25 °C. NOESY spectra were used to trace through space connectivities and to obtain chemical shifts of all ^1H resonances. TOCSY (80 and 160 ms isotropic mixing times), DQF-COSY, and COSY-35 data were obtained with parameters identical to those used for the NOESY experiments. A proton-detected $^1H-^{31}P$ COSY spectrum was obtained at 25 °C with a 2.2 s relaxation delay. The sweep width was 2000 Hz centered at the HOD

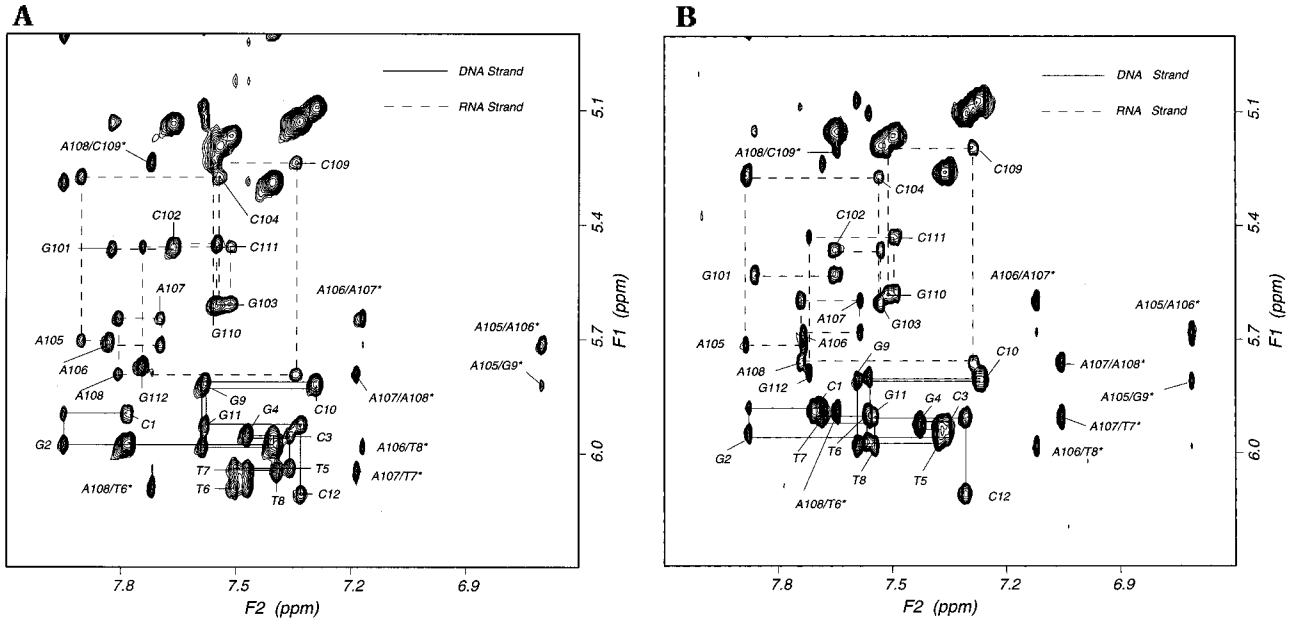

FIGURE 2: Comparison of NOESY spectra (200 ms mixing time, recorded at 25 °C) in the region of base (F2 axis) and H1′ (F1 axis) resonances for RII (A) and RIII (B). Sequential connectivities between the H1′ of the *i* residue with its own base proton (cross peaks labeled with residue numbers) and to its neighboring $i + 1$ base proton in the duplexes are linked with solid lines for the DNA strands and dashed lines for the RNA strands. NOEs between adenine H2 protons and adjacent H1′ protons on the same strand and on the complementary strand are indicated by * (A105/A106*, A105/G9*, etc.).

resonance in the ^{1}H dimension (F2) and 1200 Hz (4.55 ppm) centered at −3.39 ppm in the ^{31}P dimension (F1). A 90° phase-shifted sine bell was used in the t_2 and t_1 dimensions of NOESY spectra, while a 0° or 30° phase-shifted skewed sine bell was used prior to Fourier transformation of various COSY spectra.

COSY-35 experiments allow the direct evaluation of $J_{1'-2'}$ and $J_{1'-2''}$ by measuring the separation (in Hz) between antiphase or inphase multiplets along the resonance frequency of H1′ protons, while the passive coupling components in these cross peaks have been suppressed. The accurate measurements of $J_{3'-2'}$, $J_{3'-2''}$, and $J_{3'-4'}$ are prohibited because the ambiguities from passive coupling are still too significant in the these multiplets. However, qualitative analysis of the intensities of the cross peaks due to H3′−H2′ ($I_{H3'-H2'}$), H3′−H2″ ($I_{H3'-H2''}$), and H3′-H4′ ($I_{H3'-H4'}$) couplings in COSY-35, DQF-COSY, and TOCSY spectra provides the relative *J* values for these spin pairs. Cross peaks with greater intensity usually are associated with larger *J* coupling constants.

Three-Dimensional NOESY−NOESY Experiments. The three-dimensional (3D) NOESY−NOESY experiments for RII and RIII were performed in D_2O at 25 °C according to a previously described procedure (Boelens *et al*., 1989; Gao & Jeffs, 1994b). The 3D spectrum covered a spectral width of 5.1 kHz in each of the three dimensions and was recorded with 200 ms of NOE mixing times in both steps of magnetization transfer and a relaxation delay time of 2.9 s. The data set consisted of 2048 × 100 × 220 complex points in the F_3, F_2, and F_1 dimensions, respectively. A 90° phase-shifted sine bell function was applied to all three dimensions to give a final matrix containing 1024 × 256 × 256 data points. The 3D spectra were analyzed mainly through the planes of interest, which intersect, at resonance frequencies of base and H1′, with the F_3 axis, in order to resolve resonances overlapped in the 2D spectra, especially those involving the 2′, 3′, and 4′ protons of the RNA strands.

UV Melting Experiments

The thermal melting properties of DI−III and RI−III were examined utilizing Varian Cary 1E and 3E spectrophotometers. To obtain strictly comparable results, the experiments for the six duplexes were undertaken in parallel. Concentrated samples were diluted in the aqueous pH 6.2 buffer used for NMR experiments to give 1.0−1.1 absorption readings at 260 nm in 10 mm path length cells (∼11 μM total single strand concentration). Samples were heated from 20 to 90 °C and then cooled to 20 °C at a rate of 0.5 °C/min. The melting cycle measurements were repeated at least three times. The reported melting temperature (T_m) values are derived from hyperchromicity curves using a two state, single strand to duplex transition model. $\Delta G_{37°C}$ (abbreviated ΔG) values were derived from the UV melting curves by the nonlinear least-square fitting algorithm implemented in the Meltwin program (Petersheim & Turner, 1983). The reported T_m (±0.5 °C) and ΔG (±10%) values are average values of several experimental data sets.

RESULTS

In the following discussion we describe NMR studies of two RNA·DNA hybrid duplexes containing a single FMA or 3′-TFMA backbone linker (RII and RIII) and UV melting experiment studies of six related duplexes (DI−III and RI−III, sequences shown in Figure 1). The NMR results are examined, with reference to the RI and DI−III duplexes (Gao *et al*., 1992; Gao & Jeffs, 1994a,b).

NMR Spectra of RII and RIII

A set of 2D and 3D NOESY and COSY spectra was recorded for the RII and RIII duplexes. The exchangeable and non-exchangeable proton resonances of the two duplexes were assigned as described previously (Gao & Jeffs, 1994b). ^{31}P resonances of the two duplexes were observed in a narrow

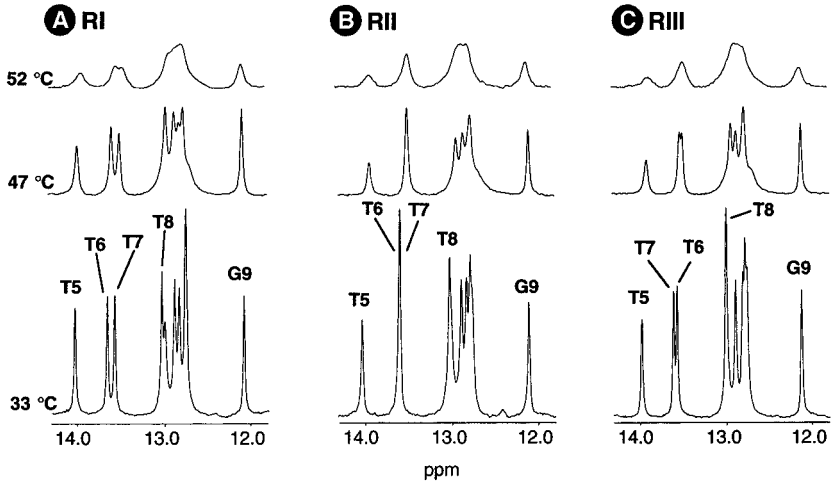

FIGURE 3: Selected one-dimensional imino proton spectra as functions of temperature for (A) RI, (B) RII, and (C) RIII. Experimental conditions and procedures are given in Materials and Methods. These spectra demonstrate that these three hybrid duplexes exhibit similar melting behavior and their melting is cooperative.

Table 1: Proton Chemical Shifts of RII and a Comparison with the Chemical Shifts of RI[a]

	DNA strand									RNA strand						
	H1/H3/$H4_b$/$H4_n$[b]	H8/H6	H2/H5	H1′	H2′	H2″	H3′	H4′		H1/H3/$H4_b$/$H4_n$[b]	H8/H6	H2/H5	H1′	H2′	H3′	H4′
dC1 δ		7.78	5.98	5.90	2.02	2.47	4.66	4.08	rG101 δ	12.76	7.82		5.46	4.59	4.40	4.15
$\Delta\delta1$[c]		0.09	0.09	0.01	−0.05	0.01	0.01	0.03	$\Delta\delta2$[c]	0.04	−0.03		−0.06	−0.04	−0.03	−0.05
dG2 δ	12.97	7.95		5.98	2.69	2.73	4.90	4.36	rC102 δ	8.31, 6.78	7.66	5.14	5.45	4.52	4.45	4.36
$\Delta\delta1$	0.02	0.06		0.02	0.06	0.01	0.01	0.02	$\Delta\delta2$	0.03, **0.37**	0.02	−0.01	−0.01	0.00	0.01	0.00
dC3 δ	8.28, 6.43	7.40	5.29	5.95	2.45	2.53	4.73	4.26	rG103 δ	12.81	7.55		5.61	4.46	4.40	4.28
$\Delta\delta1$	−0.04, −0.01	0.03	0.02	0.00	0.06	0.02	0.00	0.02	$\Delta\delta2$	−0.01	0.02		0.01	0.02	**−0.11**	−0.10
dG4 δ	12.76	7.47		5.95	2.53	2.69	4.68	4.29	rC104 δ	8.12, 6.69	7.54	5.19	5.28	4.45	4.40	4.34
$\Delta\delta1$	0.05	0.02		0.01	0.04	0.01	−0.01	0.01	$\Delta\delta2$	0.00, 0.02	0.03	0.01	0.02	0.00	0.03	0.01
dT5 δ	14.09	7.36	1.16	6.04	2.26	2.61	4.77	4.26	rA105 δ		7.90	6.70	5.70	4.47	4.63	4.41
$\Delta\delta1$	0.00	0.04	0.02	0.00	0.06	0.01	0.00	0.01	$\Delta\delta2$		0.02	0.08	0.02	0.00	**0.23**	
dT6 δ	13.68	7.50	1.52	6.09	2.23	2.77	4.44	4.17	rA106 δ		7.83	7.17	5.72	4.46	4.62	4.42
$\Delta\delta1$	−0.07	0.04	0.01	0.01	0.02	**0.15**	**−0.39**	−0.03	$\Delta\delta2$		0.05	0.09	0.05	0.05	0.04	**−0.12**
dT7 δ	13.68	7.47	1.52	6.05	2.17	2.61	4.85	4.18	rA107 δ		7.70	7.19	5.65	4.42	4.55	4.08
$\Delta\delta1$	−0.01	0.03	−0.03	0.00	0.02	0.01	0.04	−0.01	$\Delta\delta2$		−0.06	0.05	−0.01	0.02	0.03	
dT8 δ	13.08	7.39	1.61	5.98	2.31	2.56	4.89	4.19	rA108 δ		7.81	7.72	5.80	4.42	4.54	
$\Delta\delta1$	−0.03	0.03	0.02	0.02	0.03	0.02	0.02	0.02	$\Delta\delta2$		−0.02	0.06	0.02	0.02	0.09	
dG9 δ	12.07	7.59		5.82	2.47	2.57	4.86	4.31	rC109 δ	−[d]	7.34	5.13	5.24	4.29	4.33	
$\Delta\delta1$	0.02	0.04		0.02	0.04	0.02	0.01	0.02	$\Delta\delta2$	−	0.01	0.01	0.04	0.03	0.03	
dC10 δ	8.13, 6.24	7.29	5.09	5.83	2.24	2.45	4.71	4.18	rG110 δ	12.71	7.56		5.61	4.33	4.52	
$\Delta\delta1$	−0.01, 0.05	0.03	0.03	0.02	0.04	0.02	0.02	0.02	$\Delta\delta2$	**−0.14**	0.05		0.03	0.04	0.01	
dG11 δ	12.97	7.58		5.93	2.46	2.64	4.79	4.28	rC111 δ	8.31, 6.78	7.51	5.17	5.46	4.18	4.41	
$\Delta\delta1$	**0.26**	0.02		0.02	0.03	0.02	0.01	0.02	$\Delta\delta2$	−0.03, 0.07	0.02	0.00	0.02	0.10	0.01	
dC12 δ	−[d]	7.33	5.13	6.11	2.05	2.21	4.42	4.03	rG112 δ		7.74		5.78	4.22	4.28	4.20
$\Delta\delta1$	−	0.02	0.02	0.00	0.03	0.04	0.01	0.02	$\Delta\delta2$		0.02		−0.01	**0.11**	−0.01	0.03
dT6 HP1 (*pro-S*), HP2 (*pro-R*):			4.93, 5.03													
dT7 H5′ (*pro-R*), H5″ (*pro-S*):			3.70, 4.27			$\Delta\delta1$:	**−0.36, 0.15**									

[a] Nonexchangeable ^{1}H assignments were obtained from a 250 ms NOESY at 25 °C. Exchangeable ^{1}H assignments were obtained from a 150 ms NOESY at 15 °C. [b] H1 and H3 are imino protons of T and G residues, respectively. $H4_b$ and $H4_n$ are hydrogen bonded and nonbonded amino protons, respectively. [c] $\Delta\delta1$(ppm, DNA strand) = (δ, RII) − (δ, RI); comparison of the modified DNA strand with its unmodified counterparts; $\Delta\delta2$(ppm, RNA strand) = (δ, RII) − (δ, RI), comparison of the RNA strand of the modified duplex with that of the unmodified duplex. A positive value indicates that the RII duplex resonance is downfield shifted relative to that of the RI duplex. RI chemical shifts were obtained from Gao and Jeffs, 1994b. $\Delta\delta$ values larger than 0.1 ppm are highlighted in bold. [d] The four amino proton resonances belonging to dC12 and rC109 could not be unambiguously assigned because the imino proton chemical shifts on their base pair partners, rG101 and dG4, respectively, are overlapped.

0.8 ppm region. Representative NOESY spectra showing intra- and inter-residue base to sugar H1′ connectivities, typical of a right-handed duplex, of RII and RIII are given in Figure 2. The 3D NOESY−NOESY data was used to assign and to confirm assignments of the DNA and especially the RNA strand sugar protons. The H4′ of the T6 residue of RII was a key assignment that was made possible by the 3D data. The ^{1}H assignment information is summarized in Tables 1 and 2 for RII and RIII, respectively.

RII and RIII exhibit 11 Watson−Crick base-paired imino proton resonances (G H1 and T H3 protons) in the 12−14.1 ppm spectral region (Figure 3) and cytosine amino resonances of H-bonded and non-H-bonded protons in the 6.5−8.5 ppm region (Tables 1 and 2). The chemical shift differences between the ^{1}H resonances of the modified DNA strand in RII or RIII and those in the unmodified DNA strand of RI were calculated and are listed as $\Delta\delta1$ in Tables 1 and 2, respectively. These comparisons demonstrate that chemical shift perturbations due to the presence of the nonphosphate diester linker are mostly related to DNA residues T6 and T7, revealing localized conformational distortions at the FMA- or TFMA-modified site. The DNA strand in

Table 2: Proton Chemical Shifts of RIII and a Comparison with the Chemical Shifts of RI[a]

DNA strand									RNA strand						
	H1/H3/H4$_b$/H4$_n$[b]	H8/H6	H2/H5	H1′	H2′	H2″	H3′	H4′		H1/H3/H4b/H4$_n$[b]	H8/H6	H2/H5	H1′	H2′	H3′	H4′
dC1 δ		7.70	5.90	5.88	2.07	2.46	4.64	4.04	rG101 δ	12.75	7.86		5.53	4.63	4.43	4.20
$\Delta\delta$1[c]		0.01	0.01	−0.01	0.00	0.00	−0.01	−0.01	$\Delta\delta$2[c]	0.03	0.01		0.01	0.00	0.00	0.00
dG2 δ	12.96	7.88		5.95	2.64	2.69	4.88	4.33	rC102 δ	8.35, 6.72	7.65	5.15	5.46	4.53	4.44	4.36
$\Delta\delta$1	0.01	−0.01		−0.01	0.01	−0.03	−0.01	−0.01	$\Delta\delta$2	0.07 ,**0.31**	0.01	0.00	0.00	0.01	0.00	0.00
dC3 δ	8.31, 6.44	7.37	5.26	5.92	2.42	2.49	4.72	4.23	rG103 δ	12.85	7.53		5.61	4.45	4.40	
$\Delta\delta$1	−0.01, 0.00	0.00	−0.01	−0.03	0.03	−0.02	−0.01	−0.01	$\Delta\delta$2	0.03	0.00	0.01		0.01	**−0.11**	
dG4 δ	12.75	7.43		5.92	2.52	2.65	4.64	4.27	rC104 δ	8.16,6.71	7.54	5.19	5.27	4.45	4.39	4.33
$\Delta\delta$1	0.04	−0.02		−0.02	0.03	−0.03	−0.05	−0.01	$\Delta\delta$2	0.04,−0.06	0.03	0.01	0.01	0.00	0.02	0.00
dT5 δ	14.05	7.38	1.13	5.97	2.38	2.58	4.72	4.22	rA105 δ		7.88	6.71	5.72	4.48	4.62	4.39
$\Delta\delta$1	−0.04	0.06	−0.01	−0.07	**0.18**	−0.02	−0.05	−0.03	$\Delta\delta$2		0.00	0.09	0.04	0.01	**0.22**	
dT6 δ	13.66	7.57	1.51	5.89	2.50	2.60	3.48	4.07	rA106 δ		7.74	7.12	5.68	4.44	4.57	4.40
$\Delta\delta$1	−0.09	**0.11**	0.00	**−0.19**	**0.29**	−0.02	**−1.35**	**−0.13**	$\Delta\delta$2		−0.04	0.04	0.01	0.03	−0.01	**−0.14**
dT7 δ	13.71	7.68	1.48	5.91	2.20	2.56	4.67	4.19	rA107 δ		7.58	7.06	5.60	4.40	4.51	
$\Delta\delta$1	0.02	**0.24**	−0.07	**−0.14**	0.05	−0.04	**−0.14**	0.00	$\Delta\delta$2		**−0.18**	−0.08	−0.06	0.00	−0.01	
dT8 δ	13.08	7.55	1.56	5.98	2.31	2.55	4.85	4.19	rA108 δ		7.74	7.65	5.76	4.43	4.50	
$\Delta\delta$1	−0.03	**0.19**	−0.03	0.02	0.03	0.01	0.02	0.02	$\Delta\delta$2		−0.09	−0.01	−0.02	0.03	0.05	
dG9 δ	12.10	7.59		5.81	2.44	2.55	4.83	4.28	rC109 δ	−[d]	7.29	5.09	5.20	4.28	4.30	
$\Delta\delta$1	0.05	0.04		0.01	0.01	0.00	−0.02	−0.01	$\Delta\delta$2	−	−0.04	−0.03	0.00	0.02	0.00	
dC10 δ	8.18, 6.26	7.27	5.07	5.80	2.21	2.42	4.69	4.15	rG110 δ	12.79	7.51		5.58	4.30	4.51	
$\Delta\delta$1	0.04, 0.07	0.01	0.01	−0.0	10.01	−0.01	0.00	−0.01	$\Delta\delta$2	−0.06	0.00		0.01	0.00	0.00	
dG11 δ	12.96	7.56		5.91	2.43	2.62	4.78	4.26	rC111 δ	8.35, 6.72	7.50	5.16	5.43	4.07	4.40	
$\Delta\delta$1	**0.25**	0.00		0.00	0.00	0.00	0.00	0.00	$\Delta\delta$2	0.01, 0.01	0.01	−0.01		0.00	0.00	
dC12 δ	−[d]	7.31	5.10	6.10	2.02	2.16	4.40	3.99	rG112 δ		7.72	5.79	4.10	4.28	4.17	
$\Delta\delta$1	−	0.00	−0.01	−0.01	0.00	−0.01	−0.01	−0.02	$\Delta\delta$2		0.00	0.00	−0.01	−0.01	0.00	
dT6 HP1 (*pro-S*), HP2 (*pro-R*):				4.84, 5.24												
dT7 H5′ (*pro-R*), H5″ (*pro-S*):				3.54, 4.38		$\Delta\delta$1: **−0.52, 0.26**										

[a] Nonexchangeable ^{1}H assignments were obtained from a 200 ms NOESY at 25 °C. Exchangeable ^{1}H assignments were obtained from a 150 ms NOESY at 15 °C. [b] H1 and H3 are imino protons of T and G residues, respectively. H4$_b$ and H4$_n$ are hydrogen bonded and nonbonded amino protons, respectively. [c] $\Delta\delta$1(ppm, DNA strand) = (δ, RIII) − (δ, RI); comparison of the modified DNA strand with its unmodified counterparts; $\Delta\delta$2(ppm, RNA strand) = (δ, RIII) − (δ, RI), comparison of the RNA strand of the modified duplex with that of the unmodified duplex. A positive value indicates that the RIII duplex resonance is downfield shifted relative to that of the RI duplex. RI chemical shifts were obtained from Gao and Jeffs (1994b). $\Delta\delta$ values larger than 0.1 ppm are highlighted in bold. [d] The four amino proton resonances belonging to dC12 and rC109 could not be unambiguously assigned because the imino proton chemical shifts on their base pair partners, rG101 and dG4, respectively, are overlapped.

RIII displays larger changes for chemical shifts around the modification site as compared to the shifts observed in the RII duplex. The sulfur atom in TFMA causes much larger upfield shifts for the covalently linked T6 H3′ and T7 H5′,5″ resonances than the FMA group does. The comparison of the RNA strands in the three duplexes ($\Delta\delta$2, Tables 1 and 2) shows only trivial and rather scattered changes in the chemical shifts. The patterns of these changes are similar in the RNA strands of RII and RIII, indicating that the influence of the linker in the DNA strand over the complementary strand is not significant.

To evaluate the effect of hybridization when the target sequence is a DNA strand *versus* an RNA strand, DNA strand Δppm(RII−DII) ($\Delta\delta$3) and Δppm(RIII−DIII) ($\Delta\delta$4) are presented in Table 3. These values should reflect the change in chemical environment between the DNA·DNA and RNA·DNA duplexes containing the same base sequences. The majority of the $\Delta\delta$3 and $\Delta\delta$4 values fall in a range of Δppm(RI−DI) that was reported for the unmodified duplexes (Gao & Jeffs, 1994b). On the other hand, the linker related residues are more sensitive to the hybridization, and the RII and RIII duplexes were observed to respond differently ($\Delta\delta$3 and $\Delta\delta$4 differ by more than 0.1 ppm, Table 3). Another region which shows a large difference upon hybridization involves the T8 and G9 residues; the difference in chemical shift positions for the T8 and G9 imino protons between the DNA·DNA duplexes and their RNA·DNA duplex analogs is more than 0.4 ppm. These hybridization effects are present in the unmodified and the modified duplexes, suggesting that the previously observed characteristics associated with hybridization to an RNA strand persists in the modified hybrid duplexes.

Through-Bond Connectivities and Sugar Conformation of RII and RIII

The H1′−H2′ and H1′−H2″ coupling constants ($J_{1'-2'}$ and $J_{1'-2''}$) in the deoxyriboses obtained from the COSY-35 spectra are provided in Table 4. This information, in combination with qualitative assessment of the relative intensities and patterns of H3′−H2′, H3′−H2′, and H3′−H4′ coupling cross peaks in COSY-35, DQF−COSY, and TOCSY (Chary *et al*., 1987), should reveal the sugar puckers of the DNA strand residues in the two hybrid duplexes. For a C2′-endo sugar pucker, which is often associated with a B-form helix, $J_{1'-2'}$ is larger than $J_{1'-2''}$; $I_{H3'-H2'}$ (coupling cross peak intensity for H3′−H2′) is stronger than $I_{H3'-H2''}$; and $I_{H3'-H4'}$ should be weak or non-existent because of a small $J_{3'-4'}$ (J < 2 Hz). For a C3′-endo sugar pucker, which is often associated with an A-form helix, $J_{1'-2'}$ is less than $J_{1'-2''}$; $I_{H3'-H2'}$ is weaker than $I_{H3'-H2''}$; and $I_{H3'-H4'}$ is strong because of a large $J_{3'-4'}$ (J > 5 Hz). For the C2′-endo conformation the overall intensities of both H3′−H2′ and H3′−H2″ cross peaks tend to be lower than those observed for the C3′-endo conformation in a COSY-35 spectrum in which passive couplings are partially suppressed (Derome, 1987). A sugar pucker conformation in between C2′- and C3′-endo would exhibit a spectral pattern intermediate of the above two typical spectral patterns. An intermediate spectral pattern may also arise from an average of multiple conformations (Gonzalez *et al*., 1995).

Table 3: ^{1}H Chemical Shift Comparisons of the Modified DNA Strands in RII, RIII, DII, and DIII. Hybridization Effects[a]

	H1/H3/H4$_b$/H4$_n$[b]	H8/H6	H2/H5	H1′	H2′	H2″	H3′	H4′
dC1 Δδ3		0.30	0.23	0.26	0.21	0.21	0.09	0.14
Δδ4		0.20	0.12	0.22	0.24	0.17	0.05	0.05
dG2 Δδ3	0.05	0.13		0.21	0.15	0.11	0.05	0.13
Δδ4	−0.02	0.05		0.15	0.06	0.08	0.03	0.11
dC3 Δδ3	0.08, 0.09	0.20	0.03	0.38	0.54	0.23	0.01	0.19
Δδ4	0.06, 0.09	0.15	0.00	0.33	0.49	0.19	−0.01	0.15
dG4 Δδ3	−0.07	−0.31		0.03	−0.01	−0.03	−0.18	0.03
Δδ4	−0.11	−0.36		0.01	−0.03	−0.06	−0.23	−0.02
dT5 Δδ3	0.10	0.26	−0.16	0.14	0.25	0.11	0.06	0.12
Δδ4	0.13	0.24	−0.20	0.06	0.32	0.06	−0.03	0.07
dT6 Δδ3	−0.17	0.24	0.03	0.03	0.20	0.10	**−0.04**	**0.15**
Δδ4	−0.18	0.20	0.00	−0.07	0.28	0.02	**−0.15**	**0.03**
dT7 Δδ3	−0.07	**0.19**	0.01	0.08	**0.15**	0.11	0.10	0.09
Δδ4	−0.10	**0.34**	−0.04	−0.03	**0.25**	0.06	0.03	0.06
dT8 Δδ3	**−0.46**	**0.24**	0.05	0.28	0.39	0.22	0.13	0.18
Δδ4	**−0.49**	**0.33**	0.00	0.27	0.35	0.19	0.07	0.16
dG9 Δδ3	**−0.47**	−0.16		0.12	−0.06	0.04	0.01	0.06
Δδ4	**−0.45**	−0.17		0.10	−0.06	−0.01	−0.05	0.04
dC10 Δδ3	0.04, −0.06	0.11	−0.14	0.25	0.44	0.23	0.03	0.15
Δδ4	−0.05, −0.07	0.08	−0.16	0.21	0.39	0.19	−0.01	0.11
dG11 Δδ3	0.01	−0.16		0.12	−0.01	0.06	−0.05	0.08
Δδ4	−0.09	−0.21		0.09	−0.05	0.02	−0.07	0.04
dC12 Δδ3		0.08	−0.09	0.09	−0.01	0.15	0.07	0.13
Δδ4		−0.01	−0.23	0.04	−0.02	0.07	0.02	0.06
dT6 HP1 (*pro-S*), HP2 (*pro-R*):	Δδ3: **0.13, 0.09**							
	Δδ4: **−0.12, 0.25**							
dT7 H5′ (*pro-R*), H5″ (*pro-S*):	Δδ3: **0.17, 0.05**							
	Δδ4: **−0.13, 0.33**							

[a] Chemical shifts are from Tables 1 and 2 and those of DII and DIII are from Gao et al. (1992) and Gao and Jeffs (1994a). Δδ3(ppm, DNA strand) = (δ, RII) − (δ, DII); and Δδ4(ppm, DNA strand) = (δ, RIII) − (δ, DIII). A positive value indicates that the resonance of the modified DNA strands in RII or RIII is downfield shifted compared to that in the DII or DIII duplex. Δδ3 − Δδ4 > 0.1 ppm are highlighted in bold. Note the exceptionally large differences in the T8 and G9 imino proton resonances (values highlighted). [b] H1 and H3 are imino protons of T and G residues, respectively. H4$_b$ and H4$_n$ are hydrogen bonded and nonbonded amino protons, respectively.

Table 4: Coupling Constants of DNA Sugar Protons in the Hybrid Duplexes[a]

	RIII		RII		RI	
residue	$J_{1'-2'}$	$J_{1'-2''}$	$J_{1'-2'}$	$J_{1'-2''}$	$J_{1'-2'}$	$J_{1'-2''}$
dC1	6.1	6.5	7.5	7.4	6.3	6.3
dG2	7.2	6.7	6.8 (o)	7.5 (o)	7.3	6.5
dC3	6.0	6.0	7.1	5.1 (o)	7.1	5.7
dG4	6.5	6.5 (o)[b]	8.7 (o)	5.6 (o)	7.3	6.5
dT5	6.8	6.7	7.0	9.0 (o)	7.5	7.3
dT6	6.2	6.4	8.8	6.7	7.5	6.5
dT7	6.1	6.3	7.5	9.0 (o)	7.7	6.7
dT8	6.6	6.9	7.8	7.5	8.5	6.5
dG9	7.1	6.9	7.5	7.5	8.0	6.0
dC10	6.7	6.3	6.9	6.3	6.5	5.9
dG11	6.6	6.3	7.6	7.4	7.3	6.3
dC12	7.4	6.3	7.4	7.4	6.9	6.1

[a] Coupling constants were measured from COSY-35 spectra. RI $J_{1'-2'}$ and $J_{1'-2''}$ values are from Gao and Jeffs (1994b). Error estimation is ±0.5 Hz. *J* values for terminal residues are less reliable due to the inherent flexibility of these residues. [b] (o): Peaks are partially or completely overlapped, and *J* is estimated.

Based on the discussion above, we analyzed, in detail, the coupling data of the T residues, which are adjacent to the linker site, in the DNA strand of the RIII duplex, because this sequence exhibits better resolved resonances (Table 4). The corresponding RII spectral data were then examined on a comparative basis. For the T residues in RIII the COSY data reveal $J_{1'-2'}$ and $J_{1'-2''}$ of the sugar moieties in T5, T7, and T8 are about the same within experimental errors (Table 4). The $I_{H3'-H2'}$ and $I_{H3'-H2''}$ are about equal for T5, whereas for T7 and T8, $I_{H3'-H2'} > I_{H3'-H2''}$. The $I_{H3'-H4'}$ for T5, T7, and T8 are of medium intensities. Overall these data indicate deviation of these T sugar rings from the C2′-endo conformation and even an increased contribution of the C3′-endo type conformation in T5 sugar pucker compared to that in T7 and T8 sugars. For the corresponding T residues in RII, the $J_{1'-2'}$ values are consistently greater than those of RIII (Table 3). The $I_{H3'-H2'}$ and $I_{H3'-H2''}$ of RII are much lower than those of RIII, while the $I_{H3'-H4'}$ are moderately strong. These data suggest that the RII T5-T8 sugar puckers contain less contribution from C3′-endo than their counterparts in RIII. $J_{1'-2'}$ and $J_{1'-2''}$ of the G and C residues in RII and RIII are within 0.5 Hz of each other in most cases, and their H3′−H4′ cross peaks are barely detected in the COSY experiments (with the possible exception of C10 of RIII), indicating that they have $J_{3'-4'} \approx 2.5$ Hz (the resolution of the experiments in the F2 dimension). The sugar puckers of these residues of the DNA strands of RII and RIII are slightly more influenced by C3′-endo conformations than those found in standard B-form DNA.

The overall distribution of preferred sugar conformations for the DNA strand of RIII and RII is compared, through coupling constants (Table 4), with that of RI (with the exception of T6 which is discussed later). The differences between $J_{1'-2'}$ and $J_{1'-2''}$ are small in RIII (∼1 Hz), in contrast to some large differences (*e.g.*, 1.4 Hz in C3 and 2 Hz in T8 residues) observed in the RI duplex. This difference is most likely attributable to the presence of a TFMA linker in the DNA strand of RIII, which prefers a more C3′-endo conformation for the adjacent DNA residues. The coupling constants of RII are less well defined for some of the residues (Table 4), but the available data indicate that the contribution of the C3′-endo conformation within sugar puckers of the DNA strand in the three hybrid duplexes is in the order of RIII > RI ≈ RII.

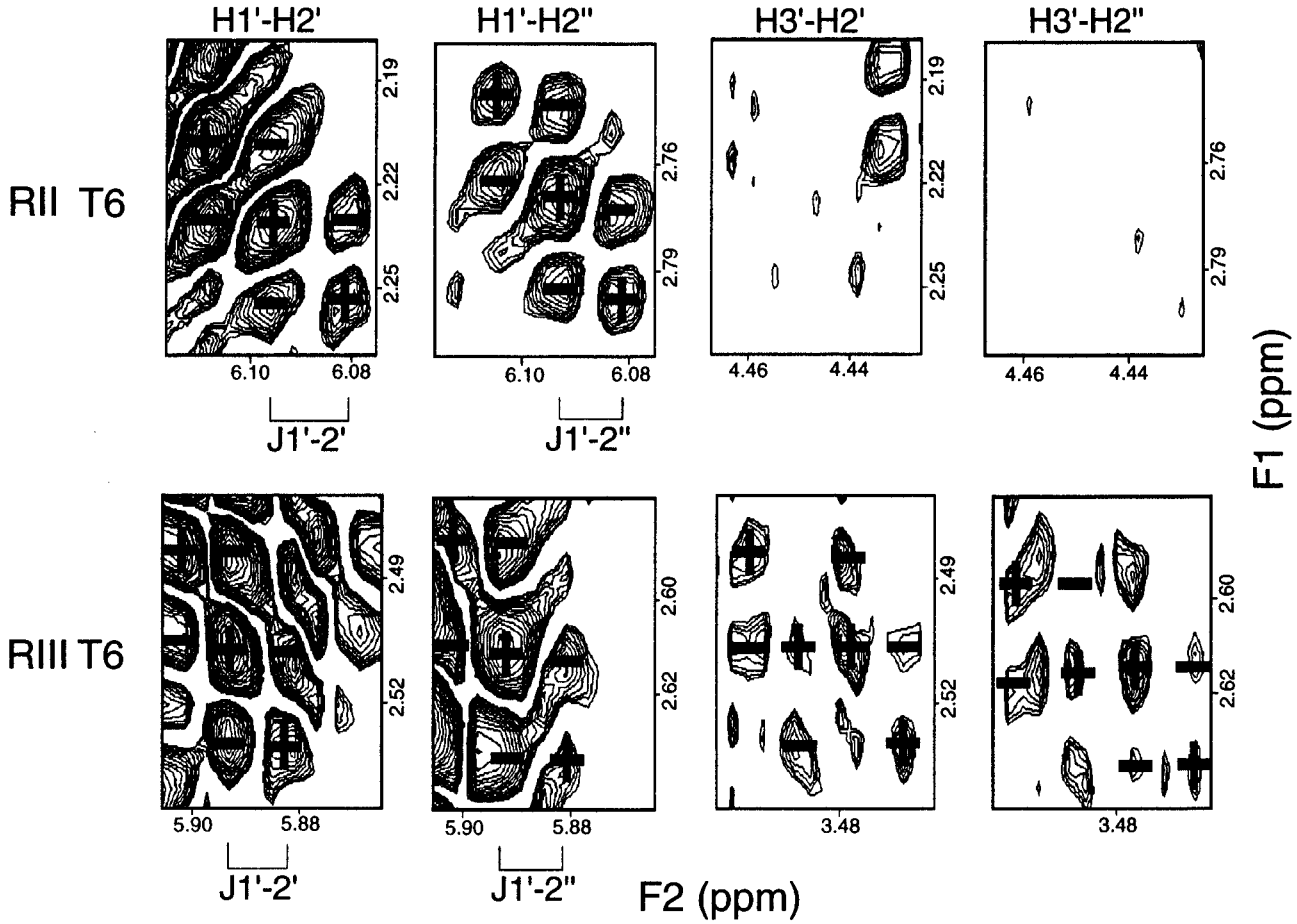

FIGURE 4: Expanded COSY-35 spectra of RII (top panels) and RIII (bottom panels) showing the H1′−H2′, H1′−H2″, H3′−H2′, and H3′−H2″ multiplet antiphase cross peaks of the T6 sugar residue. All spectra were plotted with the same spectral width "+" indicates the positive phase, and "−" indicates the negative phase of the multiplets. The cross peak connecting RII T6 H3′ and H2′ is extremely weak and that connecting H3′ and H2″ is absent.

For the RNA sugar residues of RIII or RII, with the exception of G112, H1′−H2′ cross peaks are not detected in either DQF−COSY or COSY-35 experiments, indicating $J_{1'-2'} < 2.5$ Hz. In addition, $I_{H3'-H4'}$'s are medium to strong. These data suggest that the RNA strands of RIII and RII remain in the C3′-endo type conformation when they form complementary duplexes with DNA strands containing an FMA or a TFMA linker. These results are consistent with the analysis of the RNA strand sugar conformation in the unmodified RI and other studies of natural RNA·DNA hybrid duplexes (Salazar *et al*., 1993; Gao & Jeffs, 1994a; Gonzalez *et al*., 1994). Thus, the linkers studied have little effect on the sugar pucker conformation of the target RNA strands.

Sugar Pucker of the Modified T6 Residues

The COSY-35, DQF−COSY, and TOCSY data exhibit C3′-endo characteristics that are more evident for the RIII $T6_{-TFMA}$ than RII $T6_{-FMA}$ and RI $T6_{-PO_4}$. The $J_{1'-2'}$ and $J_{1'-2''}$ of the T6 residue are nearly equal for RIII given the ±0.5 Hz error limit but are different in RII with $J_{1'-2'} = 8.8$ and $J_{1'-2''} = 6.7$ Hz (Figure 4 and Table 4) and RI with $J_{1'-2'} = 7.5$ and $J_{1'-2''} = 6.5$ Hz. Because in a standard C3′-endo conformation an H1′−H2′ cross peak would not be detected ($J_{1'-2'} < 2$ Hz), these data indicate that RIII T6 sugar pucker is not in a pure C3′-endo form, but that it contains a significant population of this form (Gonzalez *et al*., 1995). Comparatively, the RII T6 sugar pucker is more C2′-endo like than the RIII T6 sugar pucker and is closer to that of RI because its $J_{1'-2'}$ is larger than $J_{1'-2''}$ and $I_{H3'-H2''}$ is not detectable in the COSY-35 spectra unlike that of RI (Gao & Jeffs, 1994b; Figure 4 of this paper).

Overall NOE Analysis

The NOE patterns of the DNA strands containing an FMA or a 3′-TFMA modification are similar for the RII and RIII duplexes (Figure 2) and are also comparable to those of the RI duplex. A detailed analysis of the NOESY cross peak patterns of RI in comparison with the canonical B- and A-form duplexes of the same sequence has been described previously (Gao & Jeffs, 1994b). Following these analyses, the conformation of the DNA strand in RII and RIII are shown to be more close to a B-type than to an A-type helix, although deviations from canonical B-form exist. The presence of non-phosphate diester backbone linkers in RII and RIII is shown to have only minor, mainly localized effects (*vide infra*). The spectral variations from a B-form helix are detectable. For instance, in the T residues of RII and RIII, the intraresidue H6 to H3′ NOEs are medium in intensity. In contrast, the distance between these two protons in model B-form DNA would be ~4.5 Å and should give a weak to very weak NOE. On the other hand, in model A-form DNA, the distance would be 2.5−2.8 Å and would correspond to strong or medium intensity NOE peaks. Therefore, the medium intensity peaks for the T H6 to H3′ NOEs indicate that these residues are neither in a standard B- nor an A-form.

The NOE patterns of the RNA strands of RIII and RII are quite similar (Figure 2). In all three hybrid duplexes (RI−III), the RNA strand H8/H6 to H1′ NOEs are weak in intensity as expected for an A-form helix. The interresidue NOE connectivity is intact, demonstrating that hybridization to the modified DNA strands does not disrupt the normal A-type structure of the RNA strands. For the A-tract residues of RIII and RII, moderate NOEs are present between A H2 and H1′ protons of 3′ residues of the same strand ($H2_i$/$H1'_{i+1}$), while weak to moderate NOEs are present from A H2 to H1′ protons in the 3′-direction of the complementary strand ($H2_i$/$H1'_{j+1}$) (Figure 2). The relatively stronger cross strand H2/H1′ NOEs than those intra-strand NOEs reflect features of an A-type RNA. The cross strand H2/H1′ NOEs also exhibit increased intensity from A105 to A108, indicating progressively closer contacts between these proton pairs. Weak NOEs, that have about the same intensity as the H8/H6 to H1′ interresidue cross peaks, exist between A H2 protons of adjacent residues ($H2_i$/$H2_{i+1}$) for both duplexes. These NOEs are slightly stronger than what is expected for an A RNA (H2/H2 distance = 4.8 Å and H8/H6 to the sequential H1′ distance = 4.6 Å). This demonstrates that the RNA strands of RII and RIII are mostly A-form-like with co-existence of some non-A-form patterns. The only significant changes in NOE intensities in the RNA strands occur in RNA residues near the modified linkers as discussed below.

NOEs Involving Linker HP1 and HP2 Protons

The methylene protons of the FMA or the TFMA linkers (HP1 and HP2) exhibit many contacts with nearby sugar protons (Figure 5). The analysis of these NOEs and qualitative modeling using a dinucleotide unit permit the stereospecific assignments of HP1 (*pro-S*) and HP2 (*pro-R*). These linker protons provide probes for the local conformation of the modified backbone and the immediately adjacent residues, T6 and T7, in the FMA-modified RII and the TFMA-modified RIII. A comparison of the spectral regions of the 70 ms mixing time NOESY of RII- and RIII-containing NOEs to HP1 and HP2 is shown in Figure 5 and these results are summarized in Table 5. Inspection of these spectra indicates that there are major differences in the structures of RII and RIII in the linker region. These differences are reflected in several important interproton contacts. (a) Linker protons to T6 H4′: There is an absence of NOEs between T6 H4′ and HP1 or HP2 in RII, whereas in RIII there are weak NOEs from T6 H4′ to both HP1 and HP2. (b) Linker protons to T6 H3′: In RII there is a medium intensity NOE between HP2 and T6 H3′ and a weak NOE between HP1 and T6 H3′, while in RIII the corresponding NOEs are only slightly different with both NOEs in medium intensity. (c) Linker protons to T7 H5′ and H5″: In RII the NOE of HP1 and T7 H5′ (*pro-R*) is medium in intensity, whereas that between HP1 and T7 H5″ is weak in intensity. HP2 shows a weak NOE only to T7 H5′. In RIII, four cross peaks were observed correlating HP1 and HP2 with T7 H5′ and H5" with medium to weak intensities.

The NOE patterns exhibited by the FMA and 3′-TFMA linker protons in the comparison DNA·DNA duplexes (DII and DIII) have been reported previously (Gao & Jeffs, 1994a). The comparison of this information for the same modification in the context of a different complementary strand, *i.e.*, RII *versus* DII and RIII *versus* DIII, is summarized in Table 5. This analysis reveals structural requirements by the DNA or RNA strands imposed upon the modification linker site in the complementary strand. The NOE patterns of linker-backbone protons for the FMA modified RII and DII are generally similar. In contrast, significantly different NOE patterns are present for the 3′-TFMA-modified RIII and DIII. Especially, there are only weak NOEs between both linker protons and T6 H4′ in RIII, but these NOEs are strong in DIII. The relative intensities of the NOEs connecting the linker protons with T6 H3′ and T5 H5′ also vary in RIII and DIII (Table 5). The overall NOE pattern of RIII is close to those of RII and DII instead. Additionally, it is noticed that linker proton resonances in DIII are sensitive to temperature change and are resolved better at lower temperatures. This behavior was not observed

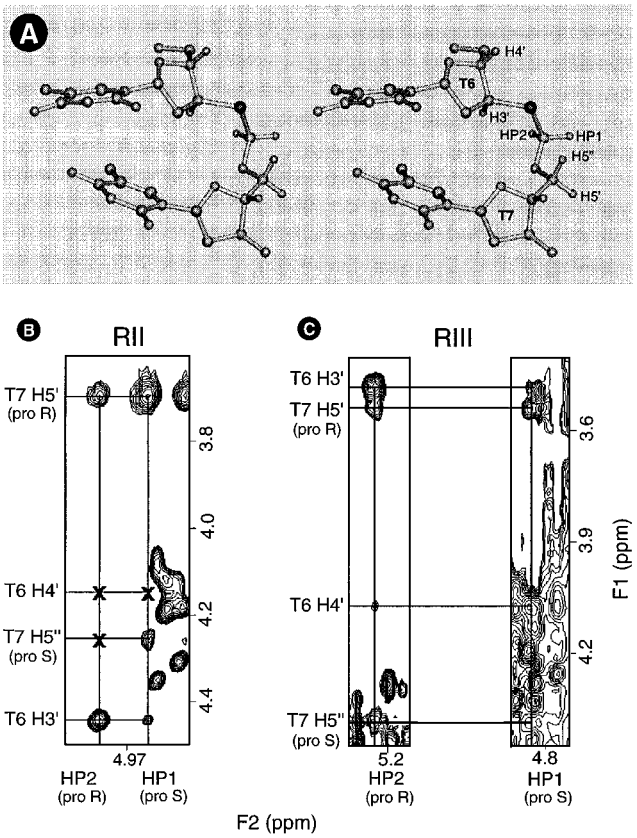

FIGURE 5: Comparison of the key NOEs involving HP1 and HP2 of RII and RIII. (A) The T6T7 dinucleotide in RIII drawn in stereopair to illustrate the linker HP1, HP2, and adjacent protons (Cross *et al.*, 1996). (B, C) 70 ms mixing time NOESY experiments recorded in D_2O at 25 °C for RII and RIII. NOE cross peaks connecting HP1 and HP2 (F2 axis) with T6 H3′, T6 H4′, T7 H5′, and T7 H5″ (F1 axis) are shown by solid lines with the corresponding resonance assignments given along the F2 and F1 axes. "X" marks the chemical shift position in two dimensions where an NOE would be expected to occur.

Table 5: NOE Comparison at the Linker Site[a]

duplex	linker CH_2	T6 H3′	T6 H4′	T7 H5′ (*pro-R*)
DIII: DNA·DNA	HP1 (*pro-S*)	w	s	w−
3′-S-CH_2-O	HP2 (*pro-R*)	w−	s−	w
RIII: RNA·DNA	HP1 (*pro-S*)	w	w	m
3′-S-CH_2-O	HP2 (*pro-R*)	m	w	w
DII: DNA·DNA	HP1 (*pro-S*)	w	nd	m
3′-O-CH_2-O	HP2 (*pro-R*)	m	nd	w
RII: RNA·DNA	HP1 (*pro-S*)	w	nd	s−
3′-O-CH_2-O	HP2 (*pro-R*)	m	nd	w

[a] NOE intensity: w, weak; m, medium; s, strong; nd, not detected.

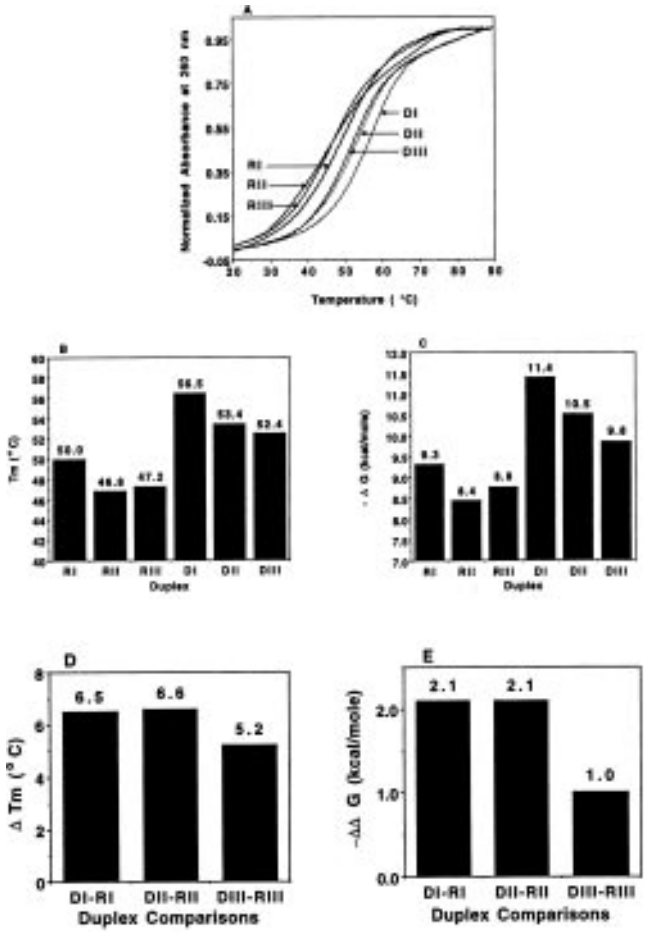

FIGURE 6: (A) Representative UV melting curves for both the hybrid and DNA duplexes. The absorbance at 260 nm has been normalized. (B) Comparison of the UV melting temperatures of all six duplexes derived from melting curves of each duplex. (C) Comparison of the $\Delta G_{37°C}$ values of all six duplexes obtained from fitting the UV melting curves using the Meltwin 2.1 program (Petersheim & Turner, 1983). (D) Comparison of the T_m differences between DNA·DNA and RNA·DNA duplexes containing the same linker between T6 and T7. (E) Comparison of the $\Delta G_{37°C}$ differences between DNA·DNA and RNA·DNA duplexes containing the same linker between T6 and T7.

in the RIII duplex, which exhibits two well-resolved linker proton resonances at all temperatures used in this study.

Temperature Dependent UV and NMR Experiments

The UV hyperchromicity of all three hybrid duplexes (RI−III) was measured and is displayed in Figure 6A. The melting curves show a generally cooperative process and the UV-derived T_m's of both RII and RIII are about 3 °C less than that of RI, although the T_m of RIII is slightly higher than that of RII (Figures 6A,B). The ΔG values (Figure 6C) derived from the UV melting data (Petersheim & Turner, 1983) follow the same pattern as the T_m's with RII and RIII being less stable to about the same degree as compared to RI.

For comparison purposes, the UV measurements for the three DNA·DNA duplexes (DI-DIII) were also carried out using a similar set of experimental conditions (Figure 6A). T_m's derived from these UV data (Figure 6B) are consistent with what was reported previously (Gao *et al*., 1992; Gao & Jeffs, 1994a). The stability of these duplexes decreases in order of DI > DII > DIII. The ΔG values (Figure 6C) also indicate that DIII is the least stable of the three DNA·DNA duplexes.

When RNA·DNA hybrid and DNA·DNA duplexes are compared, the hybrid duplexes exhibit broader UV transitions and are always less stable than their DNA·DNA counterpart by 5.2−6.6 °C in T_m or by 1.0−2.1 kcal/mol in ΔG (Figures 6D,E). The destabilization effect in the hybrid duplexes appears to be the smallest in the 3′-TFMA-modified duplexes (ΔT_m and $\Delta\Delta G$ in Figure 6D,E).

The local melting behavior of each individual base pair was monitored by NMR imino proton line broadening at elevated temperatures for the three hybrid duplexes RI−III to give sharp temperature transitions (Figure S1 of the Supporting Information). These experiments complement the information on global melting obtained from UV melting profiles. In NMR experiments, the imino peaks for T6 and T7, which are linked by the FMA or TFMA linkers, broaden at the same time as other imino protons broaden (Figure 3). T5 and G9 imino protons are well-resolved; the temperature values of their transitions points are the basis for the NMR melting temperature ($T_{m,NMR}$), which is 52 ± 1 °C for RI. The linker containing hybrid duplexes (RII and RIII) melt at about 1 °C lower temperatures than that of the unmodified RI. The NMR melting of the three hybrid duplexes follows a similar trend to that of the UV melting, but the T_m difference between the modified and the unmodified duplexes is slightly smaller in the NMR results.

For the three related DNA·DNA duplexes, the microscopic melting behavior of the linker sites were compared based on the imino proton signal broadening. In these duplexes all Watson−Crick base paired imino protons disappeared simultaneously. There is significant difference in the imino proton melting transition temperatures. In DI, the marker T8 and G9 imino protons melt out at 54 ± 1 °C, while in DII they melt out at 52.5 ± 1 °C compared to 51 ± 1 °C in DIII. These results agree well with the trend observed in the UV melting experiments, with the NMR T_m's about 1 or 2 °C lower than the UV T_m's.

DISCUSSION

Overall Structural Characterization and Stability

The NMR spectral comparisons of the modified RII and RIII duplexes with the unmodified RI duplex (Gao & Jeffs, 1994b), which include comparisons of the differences in chemical shifts, sugar proton couplings and NOE spectral data, indicate that the presence of a modified backbone linkage in RII and RIII do not cause major spectral variation. Similar to the RI duplex, the conformation of the RII and RIII duplexes are heterogeneous and characterized by DNA strands that are more B-form like and RNA strands that are more A-form like. Furthermore, the recognition of the DNA and RNA strands are compromised by the adoption of some non-A and non-B helical conformations, as reflected in varied NOE intensities and the *J* values of sugar protons compared to those of canonical A- or B-form structures. These results further demonstrate a general conformational preference of RNA·DNA duplexes to be in a hybridized form, in agreement with what has been reported in the literature (Salazar *et al*., 1993; Ratmeyer *et al*., 1994; Gonzalez *et al*., 1995). The NOE patterns characteristic of the A_4·T_4-tract are similar in the three hybrid duplexes (RI−III), suggesting that backbone modifications in this region do not disrupt the groove structure of consecutive A residues in an RNA strand.

The UV T_m and ΔG data and the NMR melting of all six duplexes (Figures 6) indicate that these duplexes melt cooperatively and that the unmodified DNA·DNA duplex is the most stable. The modified DNA·DNA duplexes are more stable than their hybrid duplex counterpart and the helical stability decreases in order of DI > FMA-DII > 3′-TFMA-DIII > RI > 3′-TFMA-RIII ≈ FMA-RII. A single FMA modification causes about 3 °C drop in T_m or 0.9 kcal/mol loss in ΔG in both DNA·DNA or RNA·DNA duplexes (comparison of DII with DI or RII with RI in Figures 6B,C). This shows that the destabilization effects of the FMA linker in the two types of duplexes are about the same. In contrast, the 3′-TFMA linker destabilizes the DNA·DNA duplex (4 °C drop in T_m or 1.6 kcal/mol reduction in ΔG, DIII *versus* DI) more than the RNA·DNA duplex (3 °C drop in T_m or 0.5 kcal/mol in ΔG, RIII *versus* RI) (Figure 6B,C).

The energy differences due to hybridization have been compared. The energy cost for the unmodified RNA·DNA hybrid duplex RI is 6.5 °C drop in T_m or 2.1 kcal/mol in ΔG when compared with the unmodified DNA·DNA duplex DI (Figure 6D,E). The FMA-modified pair of duplexes RII and DII exhibit parallel behavior [ΔT_m(DII−RII) = 6.6 °C; $\Delta\Delta G$(DII−RII) = 2.1 kcal/mol]. The energy gap is smaller for the 3′-TFMA modified duplexes RIII and DIII with a ΔT_m = 5.2 °C and $\Delta\Delta G$ = 1.0 kcal/mol. If taking the destabilization of the hybrid duplexes in general (the differences between RI and DI) into consideration, the 3′-TFMA linker actually slightly stabilizes the unstable, modified RNA·DNA hybrid duplex, possibly because the 3′-TFMA linker prefers a more RNA like, A-form conformation as compared to the 3′-FMA or phosphodiester linker.

The lower T_m of the hybrid RI duplex than that of DI is consistent with what is expected based on the literature information (Ratmeyer *et al*., 1994; Lesnik & Freier, 1995). According to Lesnik and Freier, the duplex sequence in this study belongs to the type which contains a mixed composition with one strand containing an A_4-tract and the other strand containing a T_4-tract. The T_m's of this type of sequences have been shown to be lower for the RNA·DNA hybrid duplexes than the DNA·DNA duplexes.

Conformation of the FMA Linker in RII

The FMA linker in DII, which incorporates a methylene group to replace the charged PO_2^- group between T6 and T7 residues, has been characterized in detail by NMR and molecular mechanics/dynamics calculations (Gao *et al*., 1992; Veal *et al*., 1993). The conformation of the T6 sugar is observed to be predominantly C2′-endo and the backbone orientation of this linker is similar to that of a phosphate group in canonical B-DNA. In this study, the FMA linker in the RII duplex exhibits NOESY and COSY spectral characteristics which are comparable with those observed for the FMA linker in DII, suggesting the linker conformation in RII is about the same as that in DII. The conformations of the T6 and T7 sugar moieties connected to the linker are similar in RI and RII with the T6 sugar ring containing slightly more C2′-endo character in RII than in the unmodified RI. A similar trend in sugar pucker conformation is also observed in DII and DI duplexes (Gao *et al*., 1992). These results demonstrate that the FMA linker prefers to adopt a conformation which is close to that of the canonical B-form sugar phosphate backbone in both DNA·DNA and RNA·DNA duplexes (DII and RII). This conformation [ζ (C3′−O3′−C−O5′) = ∼−90°], however, deviates from the ∼−60° energy minimum computed from model compounds by incremental rotation of the ζ equivalent torsion angle, while holding the α (O3′−C−O5′−C5′) equivalent torsion angle at −60° (Veal *et al*., 1993). This unfavorable stereoelectronic configuration is a possible structural factor which destabilizes the FMA RII duplex, although other factors, such as structural restraints imposed by the helix, van der Waals contacts, solvation, and electrostatic interactions, in concert may all contribute to the observed conformation of the FMA linker. The quantum mechanical model of the FMA linker predicts a destabilization energy of 1−3 kcal/mol for rotation of C−O−C−O angle from −60 to −90° (Veal *et al*., 1993), in agreement with the 2.1 kcal/mol difference between the ΔG values of RI and RII derived from the UV melting experiments (Figure 6C).

Conformation of the 3′-TFMA in RIII

The sugar and backbone conformations of 3′-TFMA-modified DIII are drastically different from those presented by FMA in DII (Gao & Jeffs, 1994a). The 3′-TFMA linker between the T6 and T7 residues in DIII is associated with an increased contribution from C3′-endo sugar pucker and the adoption of unusual backbone torsion angles (Gao & Jeffs, 1994a; Veal & Brown, 1995) compared to those observed in DII. In this study, the TFMA linker in the RIII duplex exhibits a COSY spectral pattern, which is similar to that observed for the TFMA linker in DIII, suggesting that the T6 sugar conformational equilibrium of RIII is also shifted toward C3′-endo puckers. The NOESY spectral characteristics for the TFMA linker of RIII are somewhat different from those observed in DIII, suggesting a different backbone conformation in RIII compared to that in DIII. Comparisons of the TFMA proton related NOEs with those expected for a canonical backbone conformation indicate that the TFMA linker torsion angles in RIII fall in a range closer to what is expected for canonical A- or B-DNA. The difference in backbone conformations between DIII and RIII should reflect the structural requirement when an antisense DNA strand hybridizes with a DNA or an RNA strand. The 3′-TFMA linker in a DNA strand is better accommodated when hybridized with an RNA strand to form a hybrid RNA·DNA duplex. This may be because the conversion of the T6 sugar from a C2′-endo like conformation to one that is more C3′-endo like is more favorable in the hybrid duplex as compared to the DNA·DNA duplex. In the hybrid duplex, all of the DNA sugar moieties appear to have more C3′-endo character, especially in the T-tract of the DNA strand (Table 4), than their counterparts in the DNA·DNA duplex [Table 2 in Gao and Jeffs (1994b)]. Therefore, the conversion of T6 to a more C3′-endo like sugar pucker by the 3′-TFMA group in RIII is less energetically costly (Veal & Brown, 1995). The unusual conformations observed for the 3′-TFMA moiety in DIII is a compromise between the preferred sugar and backbone conformation of the 3′-TFMA linker and the structural requirements of the DNA·DNA duplex. These conclusions can also be drawn from comparing ΔG and T_m values, which show that RIII is just as stable as RII; while, DIII is less stable than DII (Figure 6A−C and Figure S1). In fact, the TFMA linker in DIII could not find a stable form at low temperatures as demonstrated by

the broad resonances and chemical shift averaging of the methylene proton resonances of this group.

The stability of hybrid duplexes are highly sequence dependent (Lesnik & Freier, 1995). In the previous work of Jones *et al*. (1993), a hybrid duplex between a 15-mer RNA oligonucleotide and a complementary DNA oligonucleotide containing alternating 3′-TFMA and phosphodiester backbone linkers has a UV derived T_m that was 5 °C higher than that of an unmodified, comparison hybrid duplex. In contrast, RIII, which contains a single 3′-thioformacetal substitution, has a T_m that is 3 °C less than that of the unmodified RI hybrid duplex. These observations may be reconciled if we assume that there is a preference for structural homogeneity. Multiple 3′-thioformacetal substitutions may stabilize hybrid duplex formation by converting the entire substituted DNA strand to an A-type helix that can bind to a complementary RNA strand with higher affinity. On the other hand, the DNA strand of RIII retains some features of B-type helical structure, judging by the NOE patterns and *J*-coupling described above. This places the DNA strand of RIII in a higher energy state than that of the unmodified RI because of a conflict between the molecular forces wanting to remain in a B-like helix and those at the single linker site wanting to convert to a more A-like form. This structural heterogeneity in RIII may contribute to a lower T_m as compared to RI.

Structural Implications for Improved Antisense ODN Design

In this series of studies, we have examined the stability and conformation of oligonucleotides which incorporate an FMA or a 3′-TFMA linkage in replacement of the phosphodiester backbone linker in DNA·DNA or RNA·DNA duplexes. The information obtained from the characterization and comparison of these sequences provides a molecular basis for the design of the next generation of antisense oligonucleotides. Our results indicate that the conformations of a modified backbone are predominantly dependent on two requirements: the adoption of the lowest energy state for that chemical moiety and the fitting of the modification into the global structure of the target sequences. It is highly desirable that the replacement moieties of the natural groups be able to adopt a low energy conformation which mimics the conformation of the unmodified molecules. Judging by this standard, the 3′-TFMA substitution in a DNA strand drives a more RNA-like conformation that is preferred in the RNA hybridization and thus, this linker is a promising model for antisense targeting RNA sites. But the FMA linker confers a more B-DNA conformation to the modified sequence and thus, this linker is a preferred choice for DNA binding. In addition to the consideration of the local conformational preferences, the comparison of our results with related studies in literature (Jones *et al*., 1993) suggests that the distribution of the modification sites to achieve an overall homogeneous structural environment is also an important concern in optimization of antisense oligonucleotide design. Not only the local conformation but also the global structure of an antisense duplex, as a result of cumulative effect of chemical modifications, affects the RNA binding. An enhanced effect may be attained by placing linkers at the right position and by separating linkers with the right number of intervening residues, although such information for a specific linker in a specific duplex remains to be elucidated.

ACKNOWLEDGMENT

The authors are grateful for the generous chemistry support of Gilead Sciences and Glaxo Pharmaceuticals, Inc. We also thank Dr. S. Wong and T. Gornet (University of Texas Medical School, Houston) for the use of their Cary 1E UV spectrophotometer and Dr. D. H. Turner and J. McDowell for providing the Meltwin program. We are grateful to Dr. Collin Cross for producing Figure 3 for this paper and for his diligent proofreading of the manuscript.

SUPPORTING INFORMATION AVAILABLE

NMR melting profiles of the six duplexes studied (1 page). See any current masthead page for ordering information.

REFERENCES

Agrawal, S., & Iyer, R. P. (1995) *Curr. Opin Biotechnol. 6*, 12−19.
Beijer B., Sulston, I, Sproat, B. S., Rider, P., Lamond, A. I., & Neuner, P. (1990) *Nucleic Acids Res. 18*, 5143−5151.
Bennett, C. F., Chiang, M. Y., Chan, H., Shoemaker, J. E., & Mirabelli, C. K. (1992) *Mol. Pharmacol. 41*, 1023−1033.
Boelens, R., Vuister, G. W., Koning, T. M. G., & Kaptein, R. (1989) *J. Am. Chem. Soc. 111*, 8525−8526.
Brown, S. C, Thomson, S. A., Veal, J. M., & Davis, D. G. (1994) *Science 265*, 777−780.
Capaldi, D. C., & Reese, C. B. (1994) *Nucleic Acids Res. 22*, 2209−2216.
Ceruzzi, M., Draper, K., & Schwartz, J. (1990) *Nucleosides Nucleotides 9*, 679−695.
Chary, K. V. R., Hosur, R. V., Govil, G., Zu-Kun, T., & Miles, H. T. (1987) *Biochemistry 26*, 1315−1322.
Chiang M. Y., Chan, H., Zounes, M. A., Freier, S. M., Lima, W. F., & Bennett, C. F. (1991) *J. Biol. Chem. 266*, 18162−18171.
Cross, C., Rice, J. S., & Gao, X. (1996) *Biochemistry* (submitted).
Cummins, L., Graff, D., Beaton, G., Marshall, W. S., & Caruthers, M. H. (1996) *Biochemistry 35*, 8734−8741.
Derome, A. E. (1987) *Modern NMR Techniques for Chemistry Research*, pp 227−230, Pergamon Press, New York.
Eriksson, M., & Nielsen, P. E. (1996) *Nat. Struct. Biol. 3*, 410−411.
Freeman, R., Kempsell, S. P., & Levitt, M. H. (1980) *J. Magn. Reson. 38*, 453−479.
Gao, X., & Jeffs, P. W. (1994a) *J. Biomol. NMR 4*, 17−34.
Gao, X., & Jeffs, P. W. (1994b) *J. Biomol. NMR 4*, 367−384.
Gao, X., Brown, F. K., Jeffs, P., Bischofberger, N., Lin, K.-Y., Pipe, A. J., & Noble, S. A. (1992) *Biochemistry 31*, 6228−6236.
Gonzalez, C., Stec, W., Kobylanska, A., Hogrefe, R. I., Reynolds, M., & James, T. L. (1994) *Biochemistry 33*, 11062−11072.
Gonzalez, C., Stec, W., Reynolds, M. A., & James, T. L. (1995) *Biochemistry 34*, 4969−4982.
Helene, C., & Toulme, J. J. (1990) *Biochim. Biophys. Acta 1049*, 99−125.
Hoke G. D., Draper, K., Freier, S. M., Gonzalez, C., Driver, V. B., Zounes, M. C., & Ecker, D. J. (1991) *Nucleic Acids Res. 19*, 5743−5748.
Jones, R., Lin, Y.-K., Milligan, J. F., Wadwani, S., & Matteucci, M. D. (1993) *J. Org. Chem. 58*, 2983−2991.
Lesnik, E. A., & Freier, S. M. (1995) *Biochemistry 34*, 10807−10815.
Liebhaber, S. A., Russell, J. E., Cash, F. E., & Eshleman, S. S. (1992) in *Gene Regulation: Biology of Antisense RNA and DNA* (Erickson, R. P., & Izant, J. G., Eds.) pp 163, Raven Press, New York.
Manoharan, M. (1993) in *Antisense Research and Applications* (Crooke, S. T., & Lebleu, B., Eds.) pp 303−349, CRC Press, Boca Raton, FL.
Marion, D., & Wuthrich, K. (1983) *Biochem. Biophys. Res. Commun. 113*, 967−974.
Matteucci, M. (1990) *Tetrahedron Lett. 31*, 2385−2388.

Minshull, J., & Hunt, T. (1992) in *Antisense RNA and DNA* (McMurray, J. A. H., Ed.) pp 195, John Wiley and Sons, New York.
Nadeau, J. G., & Crothers, D. M. (1989) *Proc. Natl. Acad. Sci. U.S.A. 86*, 2622−2626.
Nielsen, P. E., Egholm, M., Berg, R. H., & Buchardt, O. (1991) *Science 254*, 1497−1500.
Petersheim, M., & Turner, D. H. (1983) *Biochemistry 22*, 256−263.
Plateau, P., & Gueron, M. (1982) *J. Am. Chem. Soc. 104*, 7310−7311.
Ratmeyer, L., Vinayak, R., Zhong, Y. Y., Zon, G., & Wilson, W. D. (1994) *Biochemistry 33*, 5298−5304.
Reynolds, M. A., Beck, T. A., Say, P. B., Schwartz, D. A., Dwyer, B. P., Daily, W. J., Vaghefi, M. M., Metzler, M. D., Klem, R. E., & Arnold, L. J. (1996) *Nucleic Acids Res. 24*, 760−765.
Salazar, M., Fedoroff, O. Y., Miller, J. M., Ribeiro, N. S., & Reid, B. R. (1993) *Biochemistry 32*, 4207−4215.
Sanghvi, Y. S. (1993) in *Antisense Research and Applications* (Crooke, S. T., & Lebleu, B., Eds.) pp 273−288, CRC Press, Boca Raton, Florida.
Sanghvi, Y. S., & Cook, P. D. (1993) in *Nucleosides and Nucleotides as Antitumor and Antiviral Agents* (Chu, C. K., & Baker, D. C., Eds.) pp 311−324, Plenum Press, New York.
Sanghvi, Y. S., & Cook, P. D. (1994) *ACS Symp. Ser. 580*, 1−22.
Shaw, J.-P., Kent, K., Bird, J., Fishback, J., & Froehler, B. (1991) *Nucleic Acids Res. 19*, 747−750.
Shoji, Y., Akhtar, S., Perisamy, A., Herman, B., & Juliano, R. L. (1991) *Nucleic Acids Res. 19*, 1543−1550.
Sinyakov, A. N., Lokhov, S. G., Kutyavin, I. V., Gamper, H. B., & Meyer, R. B., Jr. (1995) *J. Am. Chem. Soc. 117*, 4995−4996.
States, D. J., Haberkorn, R. A., & Ruben, D. J. (1982) *J. Magn. Reson. 48*, 286−292.
Tidd, D. M., & Warenius, H. M. (1989) *Br. J. Cancer 60*, 343−350.
Uhlmann, E., & Peyman, A. (1990) *Chem. Rev. 90*, 544−584.
Vasseur, J.-J., Debart, F., Sanghvi, Y. S., & Cook, P. D. (1992) *J. Am. Chem. Soc. 114*, 4006−4007.
Veal, J. M., & Brown, F. K. (1995) *J. Am. Chem. Soc. 117*, 1873−1880.
Veal, J. M., Gao, X., & Brown, F. K. (1993) *J. Am. Chem. Soc. 115*, 7139−7145.
Wagner, R. W. (1994) *Nature 372*, 333−335.
Woolf T. M., Jennings, C. G. B., Rebagliati, M., & Melton, D. A. (1990) *Nucleic Acids Res. 18*, 1763−1769.
Zamecnik, P. C., & Stephenson, M. L. (1978) *Proc. Natl. Acad. Sci. U.S.A. 75*, 280−284.

BI961760I